

## Why do Arginine and Lysine Organize Lipids Differently? Insights from Coarse-Grained and Atomistic Simulations

Zhe Wu, Qiang Cui, and Arun Yethiraj

*J. Phys. Chem. B*, Just Accepted Manuscript • DOI: 10.1021/jp4068729 • Publication Date (Web): 12 Sep 2013

Downloaded from <http://pubs.acs.org> on September 17, 2013

### Just Accepted

"Just Accepted" manuscripts have been peer-reviewed and accepted for publication. They are posted online prior to technical editing, formatting for publication and author proofing. The American Chemical Society provides "Just Accepted" as a free service to the research community to expedite the dissemination of scientific material as soon as possible after acceptance. "Just Accepted" manuscripts appear in full in PDF format accompanied by an HTML abstract. "Just Accepted" manuscripts have been fully peer reviewed, but should not be considered the official version of record. They are accessible to all readers and citable by the Digital Object Identifier (DOI®). "Just Accepted" is an optional service offered to authors. Therefore, the "Just Accepted" Web site may not include all articles that will be published in the journal. After a manuscript is technically edited and formatted, it will be removed from the "Just Accepted" Web site and published as an ASAP article. Note that technical editing may introduce minor changes to the manuscript text and/or graphics which could affect content, and all legal disclaimers and ethical guidelines that apply to the journal pertain. ACS cannot be held responsible for errors or consequences arising from the use of information contained in these "Just Accepted" manuscripts.



ACS Publications

High quality. High impact.

The Journal of Physical Chemistry B is published by the American Chemical Society.

1155 Sixteenth Street N.W., Washington, DC 20036

Published by American Chemical Society. Copyright © American Chemical Society.

However, no copyright claim is made to original U.S. Government works, or works produced by employees of any Commonwealth realm Crown government in the course of their duties.

1  
2  
3  
4  
5  
6  
7      **Why do Arginine and Lysine Organize Lipids**  
8  
9  
10  
11      **Differently? Insights from Coarse-Grained and**  
12  
13  
14      **Atomistic Simulations**  
15  
16  
17  
18  
19

20      Zhe Wu, Qiang Cui\*, and Arun Yethiraj\*

21  
22      *Department of Chemistry and Theoretical Chemistry Institute, University of Wisconsin-Madison,*  
23  
24      *1101 University Avenue, Madison, WI 53706*  
25  
26

27      E-mail: cui@chem.wisc.edu,yethiraj@chem.wisc.edu  
28  
29  
30  
31  
32  
33  
34  
35  
36  
37  
38  
39  
40  
41  
42  
43  
44  
45  
46  
47  
48  
49  
50  
51  
52  
53  
54  
55  
56  
57

---

58      \*To whom correspondence should be addressed  
59  
60

## Abstract

An important puzzle in membrane biophysics is the difference in the behaviors of Lysine (Lys) and Arginine (Arg) based peptides at the membrane. For example, the translocation of poly-Arg is orders of magnitude faster than that of poly-Lys. Recent experimental work suggests that much of the difference can be inferred from the phase behavior of peptide/lipid mixtures. At similar concentrations, mixtures of phosphatidylethanolamine (PE) and phosphatidylserine (PS) lipids display different phases in the presence of these polypeptides, with a bicontinuous phase observed with poly-Arg peptides and an inverted hexagonal phase observed with poly-Lys peptides. Here we show that simulations with the coarse-grained (CG) BMW-MARTINI model reproduce the experimental results. An analysis using atomistic and CG models reveals that electrostatic and glycerol-peptide interactions play a crucial role in determining the phase behavior of peptide-lipid mixtures, with the difference between Arg and Lys arising from the stronger interactions of the former with lipid glycerols. In other words, the multivalent nature of the guanidinium group allows Arg to simultaneously interact with both phosphate and glycerol groups, while Lys engages solely with phosphate; this feature of amino acid/lipid interactions has not been emphasized in previous studies. The Arg peptides co-localize with PS in regions of high negative Gaussian curvature and stabilize the bicontinuous phase. Decreasing the strength of either the electrostatic interactions or the peptide-glycerol interactions causes the inverted hexagonal phase to become more stable. The results highlight the utility of CG models for the investigation of phase behavior but also emphasize the subtlety of the phenomena, with small changes in specific interactions leading to qualitatively different phases.

## Introduction

Interactions between cationic amino acids and lipids play an important role in the function of many membrane-active peptides and membrane proteins. Cationic amino acids are essential to the localization of peripheral membrane proteins to regions enriched with specific anionic lipids (e.g., cardiolipin or Phosphatidylinositol 4,5-bisphosphate).<sup>1</sup> Arginine (Arg) residues in the volt-

age sensor domain are believed to respond to changes in membrane potential and therefore trigger the gating transition of voltage gated ion channels;<sup>2,3</sup> some models<sup>4</sup> implicate direct interaction between "snorkeling" Arg and lipids. Finally, cationic residues are richly featured in antimicrobial and cell penetration peptides.<sup>5,6</sup> It has been suggested that these cationic motifs not only help recognize anionic regions of the membrane but also are essential to the creation/stabilization of membrane remodeling, such as pore formation.<sup>7</sup> Therefore, it is important to understand the physical factors that control the strength of interaction between cationic amino acids and lipids, as well as the impact of such interaction on the (re)organization of lipids.

One particularly interesting question in this context concerns the difference between Arg and Lysine (Lys). Although both are positively charged in their physiologically relevant titration state, there is increasing evidence that they interact with the environment rather differently. For example, several computational studies<sup>8,9</sup> estimated that the penalty of transferring a charged Lys sidechain to the center of a lipid bilayer is considerably larger than that for Arg, suggesting that a Lys buried in the membrane is likely to be deprotonated while Arg remains charged.<sup>8–10</sup> This has been confirmed very recently by experiments<sup>11</sup> for the  $pK_a$  value of residues (on a transmembrane helix) expected to be surrounded by the hydrophobic region of a bilayer. The  $pK_a$  values of Lys were below 7.0 but neutral Arg was not observed between a pH of 4 and 9, suggesting that Lys is neutral and Arg is charged under physiological conditions. In a somewhat related context, although Lys residues buried in the interior of a soluble protein are often observed to undergo significant downward  $pK_a$  shifts, internal Arg residues always remain charged.<sup>12</sup> In cell penetration peptides, replacing Arg residues with Lys considerably reduces the translocation efficiency.<sup>13</sup>

It has been suggested recently that Arg is more effective than Lys in stabilizing membrane pores. In a set of striking experiments,<sup>14</sup> Wong and co-workers showed that poly-Arg and poly-Lys led to different phase behavior when mixed with 80% phosphatidylethanolamine (PE) and 20% phosphatidylserine (PS) mixtures: while poly-Lys induced an inverted hexagonal phase, poly-Arg led to a bicontinuous (double diamond) phase. Since the bicontinuous phase is rich in negative Gaussian curvature, a feature shared by membrane pores, it was suggested<sup>7</sup> that the different phase

behavior indicates that Arg is more effective at stabilizing membrane pores, which might explain the higher translocation efficiency of poly-Arg than poly-Lys.

These observed differences between Arg and Lys are often explained in terms of the chemical features of the sidechains. While the protonated amino group in Lys has localized charges, the guanidinium cation in Arg is featured with more delocalized charge distributions. More importantly, the multiple -NH groups are believed to endow guanidinium (thus Arg) the capability to form multi-dentate hydrogen bonding interactions with surrounding groups, while this is not possible with Lys.<sup>15</sup> In the context of interaction with lipids, it is believed that Arg is able to simultaneously interact with multiple lipid phosphate groups and therefore leads to an organization of lipid molecules relative to the peptide backbone such that structures featured with negative Gaussian curvature (e.g., a bicontinuous phase) are formed or stabilized.<sup>16</sup> Lacking this feature, poly-Lys is argued to favor structures with positive or zero Gaussian curvature, such as the inverted hexagonal phase. The importance of multi-dentate interactions was tested by Wender and co-workers,<sup>17,18</sup> who methylated the guanidinium group in poly-Arg and observed decrease in the translocation efficiency.

Another difference noted in the literature concerns the interaction between two Arg/Lys sidechains. While two Lys sidechains are observed to have repulsive interactions in classical MD simulations,<sup>19</sup> as expected based on simple electrostatic considerations, both classical<sup>19</sup> and ab initio<sup>20</sup> MD simulations indicated that two guanidinium groups (thus Arg) have favorable stacking interactions in solution, stabilized primarily by their amphiphilic behavior and van der Waals interactions.<sup>20</sup> These favorable interactions have been invoked to argue that poly-Arg organizes lipid molecules differently compared to poly-Lys. In a recent study,<sup>21</sup> this hypothesis was tested by designing polymers in which the separation between guanidinium groups is systematically varied. It was observed that the separation modulates the phase properties of polymer/lipid mixtures. Although the same bicontinuous phase was observed, increasing the separation between guanidinium groups increased the unit cell size and decreased the induced negative Gaussian curvature. Therefore, the correlation between Arg side chains appears to contribute to the stabilization of negative

Gaussian curvature, although the role of other interactions has not been tested.

It is becoming increasingly clear that Arg and Lys differ in their interactions with lipid molecules and therefore organize lipids differently around them. Nevertheless, it remains unclear what groups in the lipids interact most differently with Arg/Lys and precisely how peptides are partitioned between water and lipid components to stabilize distinct phases. Understanding these issues will help clarify the physical principles that govern peptide(polymer)/lipid organization and therefore provide guidance to the design of novel materials that organize lipids and other surfactants in a controlled fashion. In this study, we combine atomistic and coarse-grained (CG) simulations to analyze the interaction of poly-Arg and poly-Lys with the lipid mixtures studied in previous experimental work.<sup>14,16,21,22</sup>

We find that electrostatic interaction between the peptide and lipid head groups is essential to the stabilization of the bicontinuous phase; decreasing the magnitude of electrostatic interaction by either replacing anionic lipids such as PS with zwitterionic lipids such as phosphatidylcholine (PC) or increasing salt concentration favors the inverted hexagonal phase. Atomistic simulations indicate, however, that the peptide/phosphate-group interaction may not be the dominant difference between Arg and Lys. The key difference that we observe between Arg and Lys lies in their interaction with lipid glycerol groups, and CG simulations indicate that a strong peptide-glycerol interaction is correlated with the formation of the bicontinuous phase. Therefore, the emerging picture from the combined atomistic/CG study is that the effective multi-dentate feature of Arg indeed leads to different lipid organization compared to Lys, and this is likely because Arg is able to simultaneously interact strongly with both the phosphate and glycerol groups in lipids while Lys can not. This aspect of peptide/lipid interactions has not been noted in previous studies.

## Computational Methods

### Coarse-Grained (CG) simulations with BMW-MARTINI

#### Modified BMW-MARTINI models

The length scales in the experiments are sufficiently large, the lattice constant for the poly-Arg/Lys (Arg<sub>9</sub>/Lys<sub>9</sub>) and lipid mixtures is ~10 nm,<sup>14</sup> that a CG model is required. The highly charged nature of the peptides suggests a CG model designed to treat electrostatic effects. For these reasons, most of the CG simulations are carried out using the BMW-MARTINI model developed by us,<sup>23,24</sup> with minor changes to Lys made to better distinguish Arg and Lys (see below). To test the effect of a diffuse charge distribution, we also construct a “double-headed” model for Arg in which the side chain is represented by three sites rather than two as in the original MARTINI<sup>25</sup> and BMW-MARTINI<sup>24</sup> force fields. Finally, for comparison, simulations are also carried out with the original MARTINI model<sup>26</sup> and the Polarizable MARTINI model;<sup>27</sup> the results of simulations with MARTINI and POL-MARTINI are presented in the **Supporting Information**.

In the original BMW-MARTINI model,<sup>24</sup> the non-polar interaction between the charged side-chain bead in Lys (Q<sub>d</sub>) and lipid glycerol (N<sub>a</sub>) is the same as that for Arg (RQ<sub>d</sub>) and lipid glycerol: both interactions are characterized with a well depth of  $\epsilon = 5.6$  kJ/mol. This qualitative behavior is different from observations from our atomistic simulations, which indicate that Lys-glycerol correlation is substantially weaker than Arg-glycerol correlation (see Results). Therefore, we introduce a new bead type for the charge bead in Lysine, KQ<sub>d</sub>, which features a weaker non-polar interaction with the lipid glycerol with a well depth of 4.5 kJ/mol (detailed interaction parameters are shown in Table 1). This modification has a negligible impact on the insertion potential of mean force (PMF) of Lys into a DOPC bilayer (Fig.1b). However, the cumulative radial distribution of lipid glycerol groups around the Lys charged bead is reduced (Fig.1a). Although the degree of reduction is modest compared to the difference between Arg and Lys observed from atomistic simulations (see Results), the two Lys models lead to qualitatively different phase behaviors for the poly-Lys/lipid mixtures as described in the main text, highlighting the importance of correlation

between the amino acid and lipid glycerols to the phase behavior.

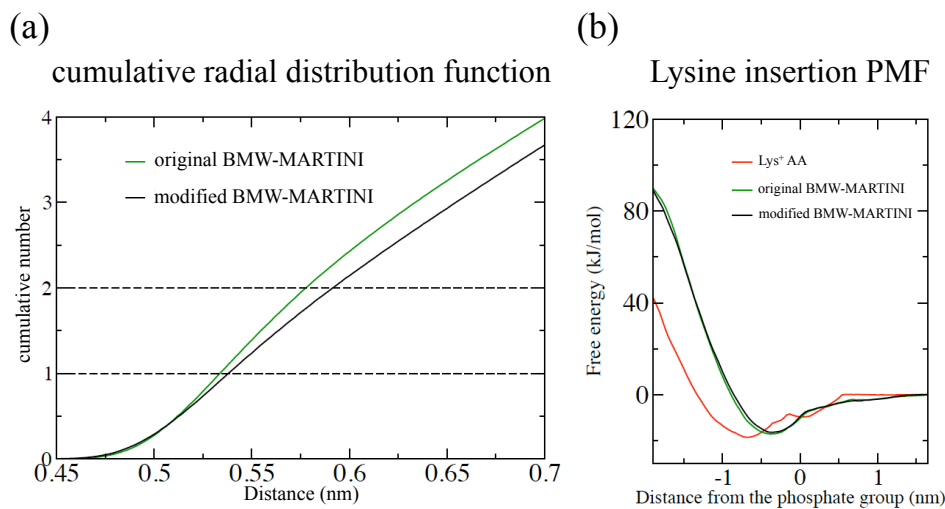


Figure 1: Comparison of properties of a Lys residue near the surface of a DOPC bilayer computed with the standard and modified BMW-MARTINI models. The modified model features a weaker non-polar interaction between the charged bead in Lys and the glycerol group in DOPC. (a) The cumulative radial distribution function of lipid glycerols around the charged bead of Lys when Lys is at its energetically most favorable location in a DOPC bilayer, i.e., -0.3 nm below lipid phosphate groups. (b) The insertion PMF for a Lysine side chain into a DOPC bilayer; the format follows that of Fig. 5 in Ref.<sup>24</sup>

In the “double-headed” CG model for Arg, the guanidine group is represented by two beads, each bearing a partial charge of +0.5, rather than one bead as in the original MARTINI<sup>26</sup> and BMW-MARTINI<sup>24</sup> models (Fig. 2a). The non-polar component for the two beads is described with a well-depth parameter of 4.48 kJ/mol, scaled by 80% based on the original BMW-MARTINI model; the distance between the two beads is restrained to be 0.23 nm, and their distances from the other side chain bead are restrained to be 0.43 and 0.47 nm, respectively, reflecting the distances among the chemical groups in an atomistic representation of Arginine. Since the charge distribution is more delocalized than the original BMW-MARTINI model, the “double-headed” Arg model leads to weaker correlation with the lipid phosphate groups in a bilayer environment (Fig. 2b); the insertion PMF into a DOPC bilayer (Fig. 2c) is very similar to that for the original BMW-MARTINI model.

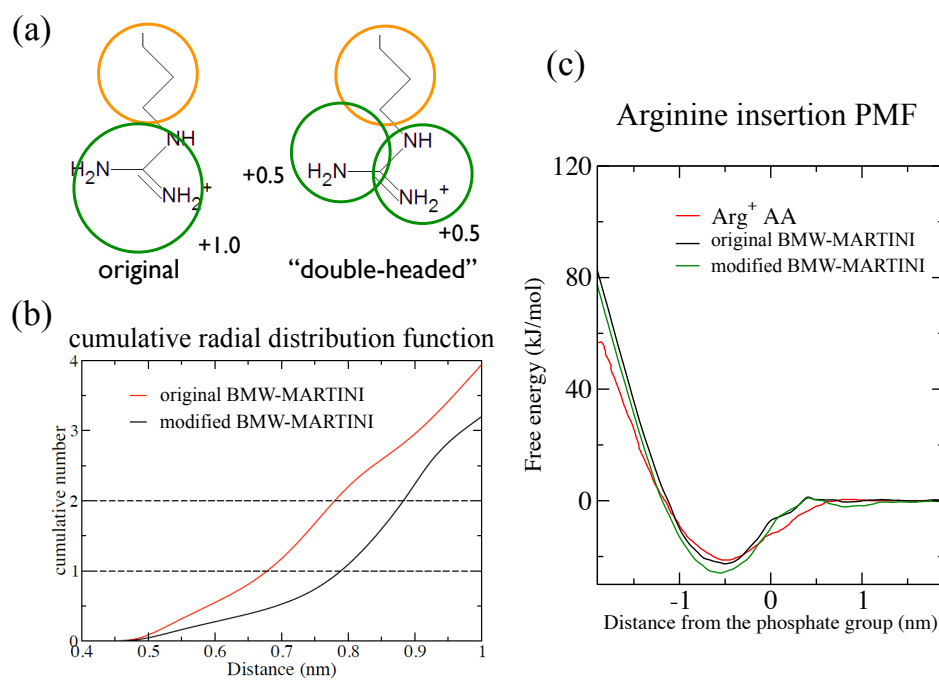


Figure 2: Development and characterization of a “double-headed” CG model for Arginine. (a) Rather than one-bead for the guanidine group as in the original BMW-MARTINI model (left), the “double-headed” model uses two CG beads, each bearing a partial charge of +0.5. (b) Cumulative radial distribution function of lipid phosphate groups around the Arginine side chain when Arg is at its energetically most favorable location in a DOPC bilayer. (c) The insertion PMF for an Arg side chain into a DOPC bilayer; the format follows that of Fig. 5 in Ref.<sup>24</sup>

Table 1: Levels of non-polar interactions among charged groups, BMW water, and uncharged groups in the updated BMW-MARTINI model.

	Q				P				N				C									
	BMW	Q <sub>da</sub>	Q <sub>d</sub>	RQ <sub>d</sub>	KQ <sub>d</sub>	Q <sub>a</sub>	AQ <sub>a</sub>	Q <sub>0</sub>	P <sub>5</sub>	P <sub>4</sub>	P <sub>3</sub>	P <sub>2</sub>	P <sub>1</sub>	N <sub>da</sub>	N <sub>d</sub>	N <sub>a</sub>	N <sub>0</sub>	C <sub>5</sub>	C <sub>4</sub>	C <sub>3</sub>	C <sub>2</sub>	C <sub>1</sub>
Q <sub>da</sub>	I	O	O	O	O	O	O	II	O	O	O	I	I	O	O	O	IV	III	III	III	III	III
Q <sub>d</sub>	I	O	I	I	I	O	O	II	O	O	O	I	I	O	III	O	IV	III	III	III	III	III
RQ <sub>d</sub>	IV	O	I	I	I	O	O	II	O	O	O	I	I	O	III	O	IV	III	III	III	III	III
KQ <sub>d</sub>	I	O	I	I	I	O	O	II	O	O	O	I	I	O	III	II	IV	III	III	III	III	III
Q <sub>a</sub>	I	O	O	O	O	I	I	II	O	O	O	I	I	O	O	II	IV	III	III	III	III	III
AQ <sub>a</sub>	I	O	O	O	O	I	I	II	O	O	O	I	I	O	O	II	IV	I	I	I	I	I
Q <sub>0</sub>	I	II	II	II	II	II	IV	I	O	I	II	III	II	II	II	II	IV	III	III	III	III	III

Level of interaction indicates the well depth in the LJ potential: O,  $\epsilon = 5.6 \text{ kJ/mol}$ ; I,  $\epsilon = 5.0 \text{ kJ/mol}$ ; II,  $\epsilon = 4.5 \text{ kJ/mol}$ ; III,  $\epsilon = 4.0 \text{ kJ/mol}$ ; IV,  $\epsilon = 3.5 \text{ kJ/mol}$ ; V,  $\epsilon = 3.1 \text{ kJ/mol}$ ; VI,  $\epsilon = 2.7 \text{ kJ/mol}$ ; VII,  $\epsilon = 2.3 \text{ kJ/mol}$ ; VIII,  $\epsilon = 2.0 \text{ kJ/mol}$ . The LJ parameter  $\sigma = 0.47 \text{ nm}$  ( $\sigma = 0.43 \text{ nm}$  for rings) is used for all interaction levels. The same grouping criteria (including subgroups) are applied as in the original MARTINI scheme. KQ<sub>d</sub> is the revised bead type for the charge particle in Lysine. The table in the previous work<sup>24</sup> is not correct due to some typos regarding the interaction levels.

### Self-assembly simulations

We perform self-assembly simulations to study the phase formed by peptide/lipid mixtures. The mixtures are simulated using GROMACS 4.5.5<sup>28</sup> starting with random placement of peptides and lipid components that eventually assemble into a stable structure with a volume of  $\sim 2000 \text{ nm}^3$ , i.e., approximately the size of two unit cells observed experimentally.<sup>14</sup> A completely anisotropic pressure coupling (triclinic box) scheme is used to allow the unit cell shape and volume to adjust during the simulation. At the beginning, a short NVT simulation at high temperature (900 K) is performed to enhance mixing. Next, at least two independent  $>6 \mu\text{s}$  simulations are performed at 300 K for each system to ensure reproducibility of the observed phases; a time step of 5-10 fs is used, which is shorter than the typical time step of 20 fs,<sup>23,24,26,29</sup> to ensure stability of the assembly simulations. Most simulations have the composition of 1024 DOPE, 256 DOPS (20% PS), 32 peptides (Arg<sub>8</sub>/Lys<sub>8</sub>, i.e., peptide:lipid = 1:40), 5120 CG water (lipid:atomistic water = 1:16) and a minimal level of NaCl for the charge neutrality of the system; several simulations with a higher concentration of NaCl are also carried out for comparison. The water to lipid ratio was not

quantitatively determined in the vesicle experiments reported in Ref.,<sup>14</sup> and 1:16 is the typical ratio that leads to the inverted hexagonal phase for pure DOPE.<sup>30</sup> The Arg/Lys peptides are modeled as extended structures without any significant secondary structure, which is supported by atomistic simulations.<sup>31</sup> We note that compared to a related study of fusion peptide/lipid mixtures,<sup>32</sup> the typical unit cell size of our systems is almost one order of magnitude larger and therefore it is too expensive to map out a detailed phase diagram. We have explored several different hydration levels between 1:12 and 1:18 and observed that the qualitative features of the simulated phase do not change significantly. Also, we emphasize that our self-assembly simulation can only claim the kinetic stability of the formed phase at  $\mu$ s time scale, but not its thermodynamic stability; since we observe consistent trends with multiple independent simulations, we interpret the assembled structures as thermodynamically stable phases.

## Analysis of phase behaviors: SAXS profiles and curvature distributions

To better compare the simulated phase to that observed experimentally,<sup>14,16</sup> we compute small angle X-ray scattering (SAXS) profiles for the assembled systems following the Fast-SAXS approach established by Roux and coworkers in which form factors for atomistic chemical groups are mapped on to CG particles.<sup>33</sup> The form factor for each CG particle needs to be determined first. Following the scheme established previously,<sup>33</sup> we estimate the form factors based on atomistic simulation of a DPPC bilayer. As shown in Eq. 1,

$$F_J^{CG}(q) = \left\langle \left| \sum_{j=1}^{n'} f_j(q) \exp(i\vec{q} \cdot \vec{r}_j) \right|^2 \right\rangle_{atom}^{\frac{1}{2}}, \quad (1)$$

we calculate the form factor curve  $F_J^{CG}(q)$  for the CG unit  $J$  with the corresponding coordinates  $\vec{r}_j$  from atomistic simulation and atomic form factors  $f_j(q)$ . The resulting CG form factor curves are fitted into quadratic forms (for  $q$  from 0.2 to 3.8 nm<sup>-1</sup>), i.e.,  $F_J^{CG}(q) = Aq^2 + Bq + C$  (shown in Fig. 3 and Table. 2), which are used in the CG SAXS profile calculations. We use the same CG

form factors for different lipid head groups (i.e., PE, PS and PC). For CG water, the topology is taken from the 4-water clusters defined in BMW.<sup>23</sup> For peptides, we map them according to the CG type definition, with guanidine/amine same as DPPC choline, other parts of the side chain as 4-carbons, and the backbone as the DPPC glycerol group.

### Form factors for Coarse-grained particles

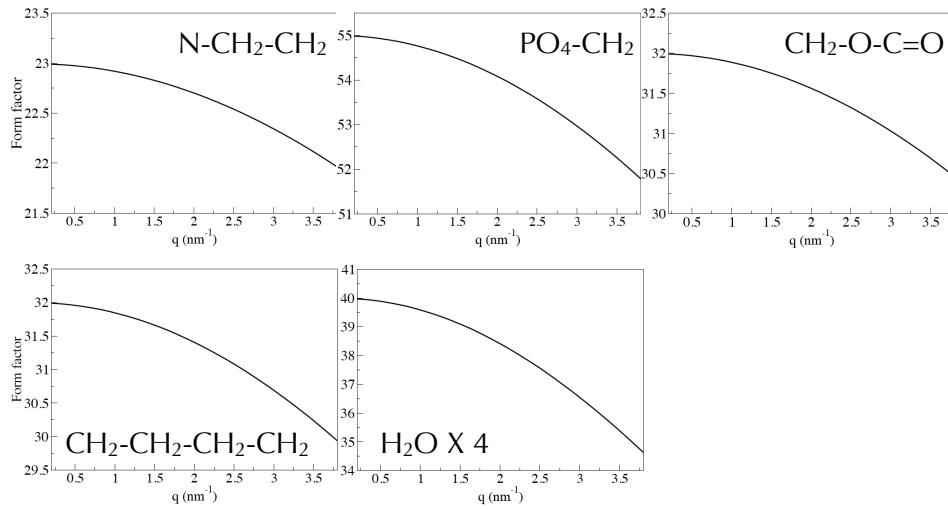


Figure 3: Form factors for different chemical groups in the coarse-grained peptide/lipid system.

**Table 2: Quadratic fitting coefficients for the coarse-grained form factor curves:**  $F_J^{CG}(q) = Aq^2 + Bq + C$ .

particle type	A (nm²)	B (nm)	C
BMW (P7)	-0.34322	-0.131534	40.0513
choline (Qd)	-0.0691931	-0.00903343	22.9963
phosphate (Qa)	-0.215502	-0.0315602	55.0087
glycerol (Na)	-0.103245	-0.0132159	32.002
4-hydrocarbon (C1)	-0.136415	-0.0282837	32.0077

The SAXS profiles for the assembled structures from the CG simulations are calculated according to Eq. 2,

$$I^{CG}(q) = \left\langle \left| \sum_{J=1}^N F_J^{CG}(q) \exp(i\vec{q} \cdot \vec{R}_J) \right|^2 \right\rangle_{CG}^{\frac{1}{2}}, \quad (2)$$

where  $I^{CG}(q)$  is the SAXS intensity,  $\vec{R}_J$  is the coordinate for CG particle  $J$  (ranging from 1 to  $N$ , where  $N$  is the total number of the CG particles). In the previous study,<sup>33</sup> the SAXS intensity includes contributions from the excluded solvent and the solvent shell at the solute boundary. Since our simulations include water molecules explicitly (although at the CG level), these terms are not necessary. The SAXS profiles are averaged over 100 snapshots from the last 1  $\mu$ s of the self-assembly simulations; each snapshot is duplicated by 27 times following the periodic boundary condition to ensure that enough number of images are included.

We also characterize the local curvature of the simulated structures. This is done by first using VMD<sup>34</sup> to obtain the triangulated mesh surface based on the density map of water, peptides and lipid head groups, with the radius scale of 5 Å for all particles, a density isovalue of 20 g/cm<sup>3</sup> (which approximately corresponds to the hydrophilic/hydrophobic interface) and a grid spacing of 5 Å. The principal curvatures  $\kappa_1$ ,  $\kappa_2$ , at each vertex on the surface are then calculated and averaged over the entire trajectory at 50 ns interval. To compute curvature around specific chemical groups, vertices within 4 Å from those groups are included.

## Atomistic simulations

Atomistic simulations are used to compare Arg and Lys regarding their local interactions with lipid molecules. For this purpose, we first compute the insertion PMF for a single Arg/Lys residue (including the zwitterionic backbone) into a DPPC bilayer. Then we analyze the lipid distributions around the sidechain when the residue is located in the bilayer at a position that corresponds to the respective PMF minimum. The Arg/Lys is described with the CHARMM22 force field<sup>35</sup> and the lipids are described with the CHARMM36 force field.<sup>36</sup> The bilayer consists of 72 DPPC molecules and the system contains 150 mM NaCl. The lipid distribution analysis makes use of ~80 ns of simulations with the Arg/Lys restrained at the respective optimal locations in the bilayer. All calculations are carried out using GROMACS 4.5.5<sup>28</sup> with NP<sub>xy</sub>P<sub>z</sub>T pressure coupling at 325 K and standard PME based non-bonded protocols.<sup>36</sup>

To probe the interaction between Arg/Lys sidechains in a membrane environment,<sup>21</sup> four copies

of cationic peptides (Arg<sub>8</sub> or Lys<sub>8</sub>) are placed on the surface of a DOPC bilayer and simulated for 400 ns at 300 K. The bilayer contains 128 DOPC lipids, thus the peptide:lipid ratio is 1:32, which is similar to that reported in Ref.;<sup>31</sup> the NaCl concentration is 150mM.

## Results and Discussion

### The importance of electrostatics in determining the phase behavior of poly-Arg/lipid mixtures

In the presence of poly-Arg, a PS-PE mixture self-assembles into a bicontinuous phase, in contrast to an inverted hexagonal phase for the same lipid mixture without the peptides. Fig.4 depicts the final snapshot of the self-assembly trajectory for the poly-Arg/PS-PE mixture at the hydration level of 1:16 using the BMW-MARTINI model.<sup>24</sup> The lipid/peptide mixture self assembles into a bicontinuous phase, in which the hydrophobic and hydrophilic components form three-dimensional networks that intersect each other. The networks are composed of mostly 4-way junctions that interconnect with each other via stalks and channels but do not fully merge as in the double diamond phase observed experimentally. This may suggest that complete convergence of the self assembly requires much longer simulations than  $\mu s$ . Nevertheless, the computed SAXS profile (Fig.5a) indicates that the assembled structure shares key scattering peaks with the phase observed experimentally.<sup>14</sup> Since the PE/PS mixture by itself assembles into an inverted hexagonal phase without the peptides (an experimental observation<sup>14</sup> reproduced with the BMW-MARTINI simulations), it is clear that the poly-Arg peptides stabilize the bicontinuous phase.

The poly-Arg and PS molecules co-localize to regions of high negative Gaussian curvature, and stabilize saddle-splay curvature. To understand the mechanism of stabilization, we characterize the distribution of poly-Arg in the assembled structure. As illustrated in Fig.6a, poly-Arg and PS lipid head groups tend to co-localize at the junction regions where channels are connected to each other to form a 3-dimensional network; these regions also feature a high degree of negative Gaussian curvature. As shown in Fig.6b, although Arg and PS head groups are observed in regions with

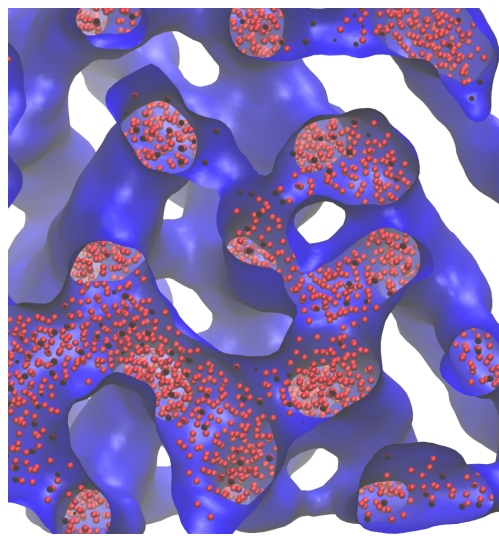


Figure 4: Final snapshot of self-assembled poly-Arg/PE/PS mixture with a hydration level of 1:16 using the BMW-MARTINI model. The density isosurface (with a value of  $20\pm5 \text{ g/cm}^3$  based on estimate with VMD<sup>34</sup>) of peptide, water and lipid head groups is shown in blue. The CG waters are shown as red spheres, and lipid tails occupy the open regions.

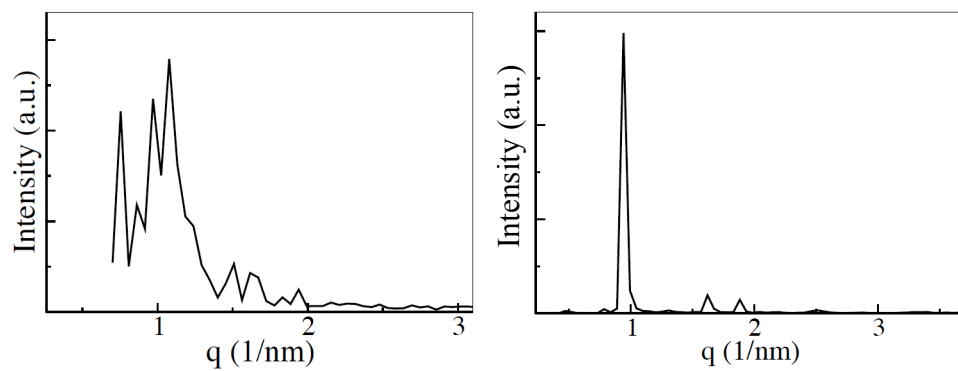


Figure 5: Computed small angle X-ray scattering (SAXS) profiles for the assembled structures for poly-Arg/PE/PS (left) and poly-Lys/PE/PS (right) with the BMW-MARTINI simulations. The qualitative features of these profiles support the interpretation that a bicontinuous phase is observed for poly-Arg/PE/PS (Fig.4), while an inverted hexagonal phase is formed for poly-Lys/PE/PS (Fig.8a), in agreement with conclusions from experimental studies.<sup>14,16</sup>

either positive or negative Gaussian curvature, they have a higher tendency than other components to localize in regions featured with large negative Gaussian curvature. Therefore, it appears that Arg and PS co-localize to stabilize saddle-splay curvature.

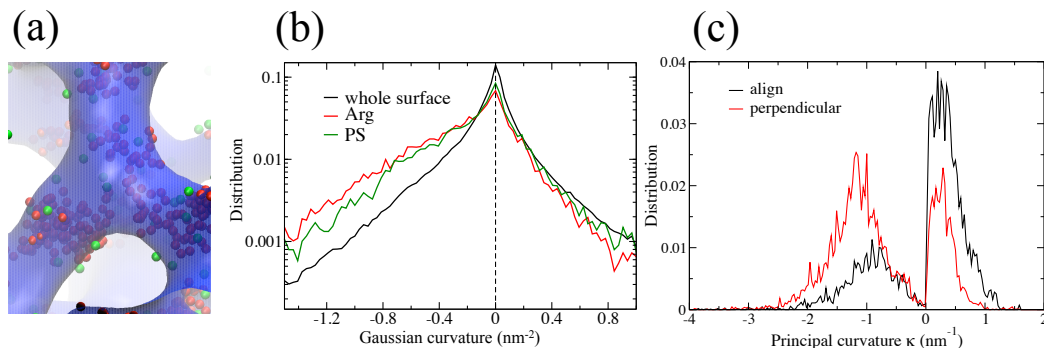


Figure 6: Poly-Arg and PS co-localize to stabilize regions with large negative Gaussian curvature. (a) A snapshot that illustrates the distribution of Arg (red spheres) and PS (phosphate represented as green spheres) near the junction region; (b) the local Gaussian curvature near (within 4 Å) the poly-Arg sidechain and PS lipid phosphate group is compared to the overall Gaussian curvature distribution in the assembled bicontinuous phase; (c) Distribution for the orientation of poly-Arg backbones relative to the principal curvatures indicate that the peptide backbone has a higher tendency to be aligned with the direction of the positive principal curvature (1-3 backbone bond vector is within 45° of the positive curvature direction) and perpendicular to the direction of the negative principal curvature.

The poly-Arg backbone has a higher tendency to be aligned with the direction of the positive principal curvature and perpendicular to the direction of the negative principal curvature (Fig.6c, also see Fig.11 for an illustration). This is a satisfying observation because (i). PE has spontaneous negative curvature,<sup>37</sup> thus poly-Arg/PS need to stabilize positive curvature to favor negative Gaussian curvature; (ii). poly-Arg peptides co-localize with PS, which has positive albeit small spontaneous curvature.<sup>37</sup> The closest sidechains, however, do not exhibit any significant preferential orientation relative to the local principal curvatures (see Fig.S1); this suggests that Arg-Arg sidechain correlations,<sup>21</sup> although contribute to, are unlikely a dominant factor for the stabilization of the bicontinuous phase (see discussions below).

The co-localization of Arg and PS head groups suggests that electrostatic interactions are essential to the stability of the bicontinuous phase. This is further supported by several additional

simulations. First, when we use the original MARTINI model<sup>25,26</sup> in which water is described as Lennard-Jones particles and the electrostatic interactions are screened by a large factor of 15, the inverted hexagonal phase is obtained (see Fig.S2 in **Supporting Information**). This occurs in both self-assembly simulations that start with random initial placements for the peptide/lipid components as well as in a simulation that starts with a snapshot of the bicontinuous phase. Second, when we lower the PS concentration to 5% in the PE/PS mixture or replace all anionic PS lipids with the zwitterionic PC lipids, the bicontinuous phase spontaneously converts into the inverted hexagonal phase. This is consistent with the experimental observation of Wong et al.,<sup>14</sup> who observed the bicontinuous phase with the poly-Arg/PE/PS mixture when the PS concentration is 20% but the inverted hexagonal phase without PS. Finally, we explore the effect of salt on the phase behavior by explicitly including salt ions in the CG simulations. As the salt concentration increases, the bicontinuous phase becomes less stable and converts to the inverted hexagonal phase with 1M of NaCl. The same effect is also seen in a set of salt-free simulations in which the real-space component of PME electrostatic interaction between Arg and all lipid head groups is scaled by a coupling parameter  $\lambda$  (note that the head group is the only charged component in a CG lipid). As shown in Fig.7, with  $\lambda = 0.8$ , the water channels that connect the junctions become large and flattened, and the final structure is an intermediate phase between inverted hexagonal and bicontinuous phases. With  $\lambda = 0.5$ , the phase resembles a tetragonal mesh phase and is featured with 2D interconnected elliptical water channels. The peptides are further away from the lipid/water interface. With  $\lambda$  smaller than 0.5, an inverted hexagonal phase is always observed.

In short, the CG simulations highlight that the electrostatic interaction between the cationic Arg sidechain and anionic lipids is essential to the formation or stabilization of the bicontinuous phase. Since both Arg and Lys are positively charged, this again begs the question: How do Arg and Lys differ in terms of their interaction with lipid molecules?

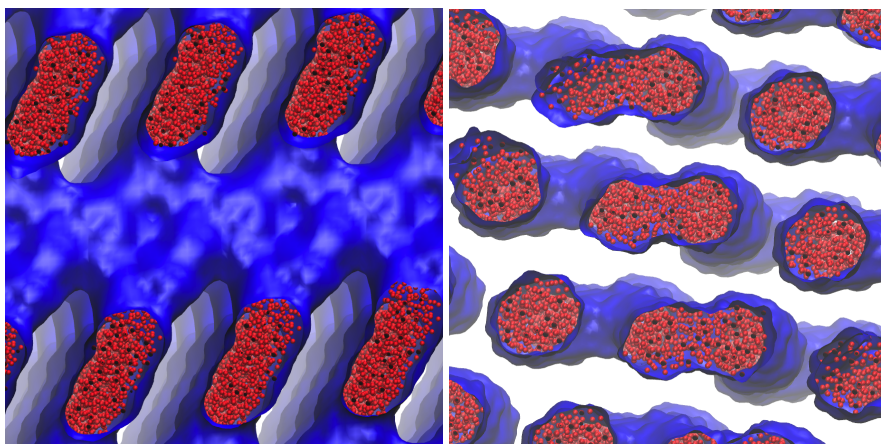


Figure 7: Self-assembled phases for the poly-Arg/PE/PS mixture when the real-space component of PME electrostatic interactions between Arg and lipid head groups are scaled by  $\lambda = 0.8$  (left) and 0.5 (right), respectively. The color scheme follows that of Fig.1.

### Differences between Arg and Lys in the context of interaction with lipids

In the presence of poly-Lys, a PS-PE mixture self-assembles into an inverted hexagonal phase, similar to what is seen without the peptides, in contrast to bicontinuous phase seen in the presence of poly-Arg. Figure 8 depicts the final snapshot of the self-assembly trajectory for the poly-Lys/PS-PE mixture at the hydration level of 1:16 using the BMW-MARTINI model. In contrast to the situation for poly-Arg (Fig.4), the inverted hexagonal phase rather than the bicontinuous phase is observed (see Fig.5 for comparison of computed SAXS profiles), in agreement with experimental observation.<sup>14</sup> In the inverted hexagonal phase, all hydrophilic components form channels that arrange hexagonally in two-dimension. Poly-Lys and PS lipids are randomly distributed within the channels and no co-localization is observed; this is further supported by the local Gaussian curvature distributions near poly-Lys and PS, which do not differ from the global Gaussian curvature distribution (Fig.8b). Since the difference between Arg and Lys is rather subtle at the CG level (see Computational Methods), additional CG and atomistic simulations are carried out to better establish the key difference between these two cationic residues that lead to distinct phases for the peptide/lipid mixtures.

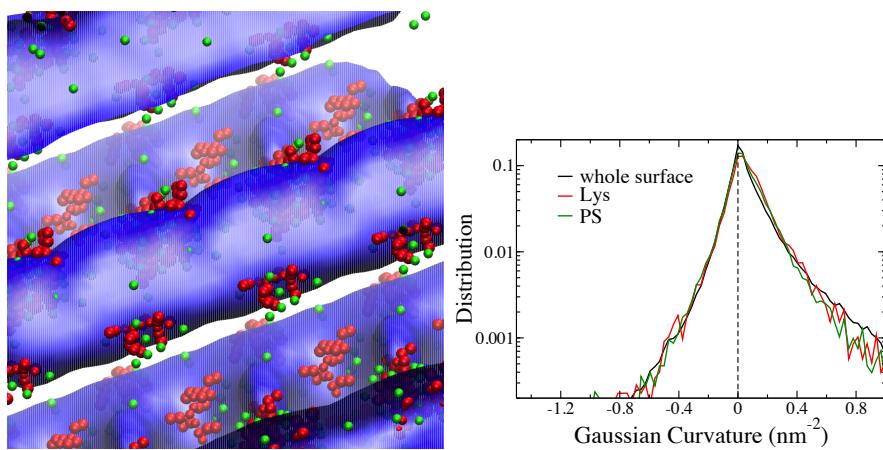


Figure 8: Poly-Lys and PS distribution in the inverted hexagonal phase formed by poly-Lys/PE/PS mixture. (left) A snapshot that illustrates the random distribution of Lys and PS in the polar channel formed by water. (right) The local Gaussian curvature near (within 4 Å) the poly-Lys sidechain and PS phosphate is compared to the overall Gaussian curvature distribution in the assembled inverted hexagonal phase. The color scheme follows that of Fig.2.

### Peptide/lipid-phosphate-group interactions are not sufficient to stabilize the bicontinuous phase

Previous studies<sup>7,16,22</sup> suggest that a potentially important difference between Arg and Lys is that Arg (unlike Lys) is able to coordinate multiple lipid phosphates through multi-dentate hydrogen-bonding interactions. Our atomistic simulations, however, indicate that Arg and Lys do not differ greatly in terms of interaction with the phosphate groups on the lipids. As shown in Fig. 9a, both residues bind effectively with one lipid head group within 4.5 Å and two within 6 Å.

To further probe the impact of amino acid-phosphate group interaction on the phase behavior of peptide/lipid mixtures, we have developed the three-bead BMW-MARTINI model for the Arg sidechain, which is featured with a more diffuse charge distribution than the original model and therefore has weaker binding affinity to lipid phosphate groups (see Fig.2). Self-assembly simulations with this new Arg model leads to qualitatively the same bicontinuous phase as with the original BMW-MARTINI model. Moreover, the inverted hexagonal phase remains to be the observed phase for the poly-Lys/PE/PS mixture when the non-polar interaction between the lipid phosphate group and Lys is increased or decreased in the CG model according to the MARTINI scales (from  $\epsilon = 5.0$  kJ/mol to  $\epsilon = 5.6$  or  $4.5$  kJ/mol). Collectively, these results suggest that a

1  
2  
3 strong interaction between peptide and the lipid phosphate group is a necessary but not sufficient  
4 condition to stabilize the bicontinuous phase.  
5  
6  
7  
8

### 9 The importance of peptide/lipid-glycerol correlations 10

11 Since Arg and Lys do not exhibit any significant difference in terms of their interaction with the  
12 lipid phosphate groups, we explore other aspects of the atomistic simulations of the bilayer system.  
13 The largest difference we observe is the pair correlation between Arg/Lys and the lipid glycerol  
14 carbonyls. As shown in Fig.9b, Arg interacts much more strongly with the glycerol carbonyl  
15 groups than Lys; within 5 Å, Arg binds almost 2 glycerol groups while Lys binds to one. Anal-  
16 ysis of configurations from the MD trajectories indicates that Arg has a 70% chance of forming  
17 a hydrogen-bond with lipid glycerol, while Lys has a chance of less than 10%; the average in-  
18 teraction between an Arg and all surrounding lipid glycerols is -55 kJ/mol, which is much larger  
19 than the value of -8 kJ/mol for Lys. Therefore, we speculate that peptide/glycerol correlation is  
20 an essential part of the effective multivalent interaction between peptide and lipids that modulates  
21 the peptide/lipid phase behavior, probably because such a correlation has a major impact on the  
22 packing of nearby lipids.  
23  
24

25 To further confirm this hypothesis, we carry out additional CG simulations for the poly-Lys and  
26 PE/PS mixtures in which the non-polar interaction between the charged bead of CG Lys and lipid  
27 glycerol bead is enhanced from “almost attractive” ( $\epsilon = 4.5$  kJ/mol) to “super attractive” ( $\epsilon = 5.6$   
28 kJ/mol). These simulations lead to a bicontinuous phase rather than the inverted hexagonal phase,  
29 highlighting the importance of amino acid-lipid glycerol interactions in determining the phase  
30 behavior of peptide/lipid mixtures.  
31  
32

### 33 The role of sidechain stacking in poly-Arg 34

35 Finally, we examine the proposal<sup>21</sup> that stacking interaction between Arg sidechains, but not be-  
36 tween Lys sidechains, plays a role in stabilizing the bicontinuous phase. Our combined atomistic  
37 and CG simulations suggest that this stacking effect likely has a minor impact on the phase behav-  
38  
39

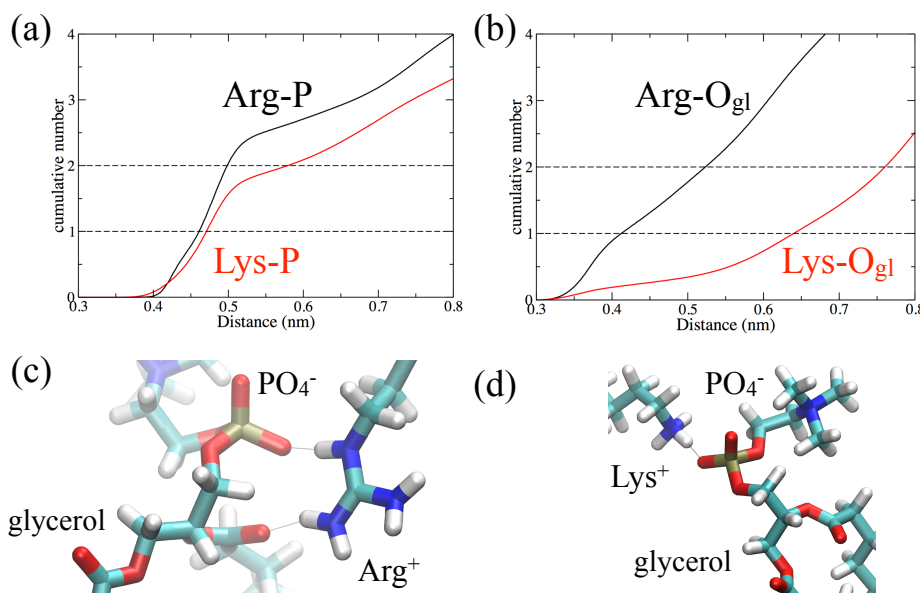


Figure 9: Cumulative radial distribution functions between Arginine/Lysine (last carbon next to the nitrogen(s) in the sidechain) and (a) lipid phosphorous (b) glycerol oxygen, at their optimal position in a DPPC bilayer (Arg: 2.06 nm; Lys 2.3 nm from membrane center). The snapshots in (c-d) illustrate that while Lys interacts predominantly with the phosphate group, Arg is able to interact simultaneously with the phosphate and glycerol carbonyl group; the latter multivalent nature of interaction is also observed in the bicontinuous phase (see Fig.S3).

ior. First, atomistic simulations of poly-Arg/poly-Lys at the surface of a DOPC bilayer (Fig.10a) reveal that although sidechain-sidechain radial distribution function (rdf) for Arg indeed has the first peak at a shorter distance ( $\sim 4 \text{ \AA}$ ) than Lys ( $\sim 6 \text{ \AA}$ ), the average sidechain/sidechain separation (i.e., the distance at which the integrated rdf reaches 1, see Fig.10b) is similar:  $\sim 8.0 \text{ \AA}$  for Arg and  $8.7 \text{ \AA}$  for Lys. Therefore, the stacking effect discussed in Ref.<sup>21</sup> based on implicit solvent and small molecule calculations is likely more subtle in a membrane/water environment due to the different configurations accessible to the sidechains. Second, due to the lower resolution representation of the sidechains, the BMW-MARTINI CG model does not capture faithfully the short-range peak in the Arg sidechain-sidechain rdf (Fig.10a). Despite this limitation, the BMW-MARTINI model leads to the bicontinuous phase for the poly-Arg/PE/PS mixture, suggesting that including the short-range stacking of Arg sidechains is not the most essential factor for stabilizing the bicontinuous phase. Finally, as mentioned above, neighboring Arg sidechains do not have any preferential orientation relative to the local curvature directions in the bicontinuous phase (see Fig.S1 in **Supporting Information**), further indicating that the contribution from Arg sidechain packing to the stabilization of negative Gaussian curvature is secondary.

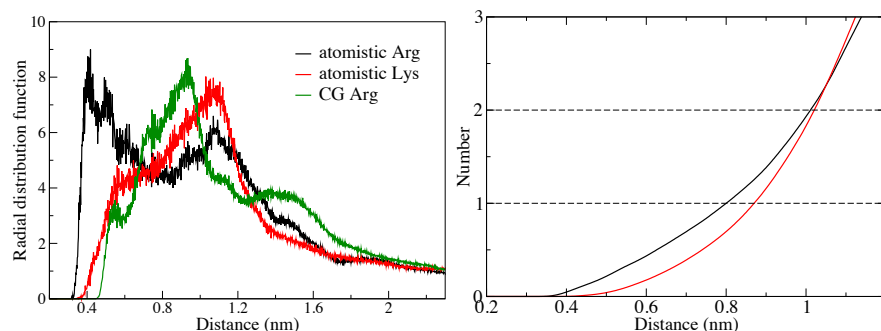


Figure 10: Comparison of Arg/Lys sidechain distributions for poly-Arg/Lys peptides on the surface of a DOPC bilayer. (left) Radial distribution functions between Arg/Lys sidechains from atomistic and CG simulations; the distances are calculated based on the last carbon in the sidechain in atomistic simulations and the last CG bead in BMW-MARTINI simulations. (right) Integrated radial distribution functions for Arg/Lys sidechains from atomistic simulations.

## Discussion: factors that lead to distinct phases for cationic peptide/lipid mixtures

In this work, we have combined atomistic and coarse-grained (BMW-MARTINI) simulations to analyze factors that lead to distinct phases for cationic peptide/lipid mixtures. In particular, we focus on the difference between poly-Arg and poly-Lys peptides, which feature the same overall charge but have been shown<sup>14,16</sup> to lead to bicontinuous and inverted hexagonal phases, respectively, when mixed with lipid mixtures that mimic the composition of bacterial membranes.<sup>38</sup> This difference in phase behavior has been suggested to reflect the ability of poly-Arg to stabilize structures with negative Gaussian curvature<sup>7</sup> such as membrane pores and therefore may explain the higher translocation efficiency of poly-Arg across the membrane than poly-Lys. Several proposals have been made regarding factors that determine the striking difference between poly-Arg and poly-Lys, although a firm conclusion has not been reached due to the limited knowledge in the distribution of the cationic peptides in the various phases.

With the BMW-MARTINI model, self-assembly simulations lead to phase behavior (Fig.4,8) in qualitative agreement with experiments for both poly-Arg/lipid and poly-Lys/lipid mixtures. The fact that distinct phases are accessible with CG models that feature a fairly low-resolution representation of the amino acid sidechains suggests that the phase behavior is not dependent on highly detailed chemical interactions, such as very directional hydrogen-bonding interactions. Rather, the CG simulations highlight the importance of electrostatic interaction (Figs.6,7) between the cationic sidechains and lipid phosphate groups in stabilizing the bicontinuous phase: the inverted hexagonal rather than the bicontinuous phase is more stable when the anionic lipid (PS in this study) concentration is reduced or salt is introduced to screen the electrostatic interaction between amino acids and lipid head groups. These observations are again consistent with experimental observations<sup>14</sup> that confirm the salt dependence of the phase behavior following suggestions from these CG simulations.

Regarding the previous hypotheses that the key difference between poly-Arg and poly-Lys is the co-ordination of Arg to multiple lipid phosphate groups<sup>14,16</sup> and the stacking interactions be-

tween neighboring Arg sidechains,<sup>21</sup> our simulation studies suggest that they don't capture the dominant mechanisms. The former was stimulated in part by the experimental observation<sup>18</sup> that methylation of Arg sidechains, which reduces their ability to form multivalent interactions, reduced the translocation efficiency of poly-Arg based peptides. The latter proposal was inspired by quantum mechanical calculations of small molecule models for Arg/Lys-phosphate interactions;<sup>21</sup> it was also supported in part by the experimental observation<sup>21</sup> that increasing the separation of Arg sidechains by inserting PEG units in the peptide main chain increased the lattice constant of the bicontinuous phase and reduced the degree of negative Gaussian curvature. Our atomistic simulations for (poly-)Arg and (poly-)Lys in a bilayer environment suggest that Arg and Lys do not exhibit major difference in terms of either interaction with lipid phosphate groups (Fig.9a) or sidechain-sidechain correlations (Fig.10), suggesting that these factors, while likely making contributions, are not the most essential to the stabilization of the bicontinuous phase. Indeed, the bicontinuous phase is obtained with the BMW-MARTINI model despite the fact that the sidechain-sidechain correlation between Arg in the BMW-MARTINI model resembles that between Lys residues from atomistic simulations (Fig.10a).

A novel observation from the atomistic simulation is that Arg and Lys differ significantly in terms of interaction with the lipid glycerol groups (Fig.9b). Evidently, the multivalent nature of the Arg sidechain allows it to coordinate simultaneously with lipid phosphate groups and glycerols, while Lys is solely engaged with the charged lipid phosphate (see Fig.9 for an illustration); as illustrated in Fig.S3, this multivalent interaction mode is also observed in the bicontinuous phase. Through interaction with the glycerol groups, Arg is able to modulate the packing of lipids and therefore the phase behavior of the peptide/lipid mixtures; this is supported by the simulation result that artificially enhancing the interaction between Lys and lipid glycerol region in CG models also leads to the formation of the bicontinuous phase.

We speculate that the mechanism for the observed phase behavior is as depicted in Fig. 11; the similar scheme was also discussed in Ref.<sup>32</sup> for understanding the phase behavior of fusion peptide/lipid mixtures. The PE and PS lipids possess negative and positive spontaneous curvature,

respectively. The charged peptides are more strongly correlated with the PS than the PE, but the stronger interaction between the Arg and glycerol groups causes a local segregation of the PS lipids with the associated Arg peptides. This segregation results in a co-localization of these species and the stabilization of regions with local negative Gaussian curvature. The stability of these regions then makes the bicontinuous phases more thermodynamically stable than the inverted hexagonal phase. The mechanism therefore relies not only on the electrostatic interactions between the peptide and lipid phosphate groups but also on the correlation between peptide and lipid glycerols.

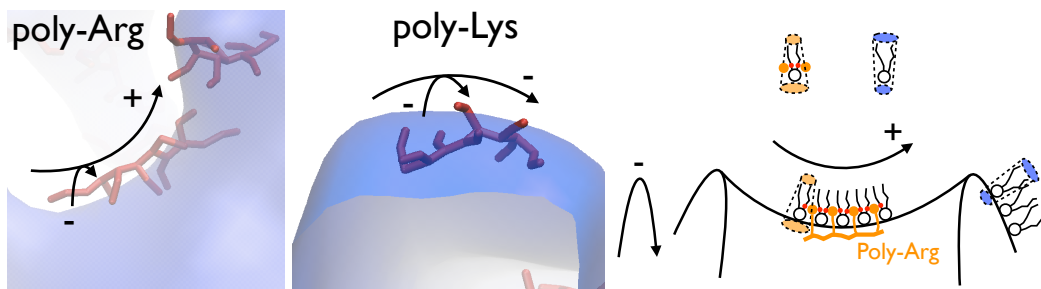


Figure 11: A scheme that illustrates our hypothesis for why poly-Arg stabilizes negative Gaussian curvature (top left) when mixed with PE/PS lipids while poly-Lys does not (top right). The blue-cone depicts PE with negative spontaneous curvature, and the orange-cones illustrate that co-localization of poly-Arg and PS further enhances the positive spontaneous curvature of PS through multiple Arg-glycerol (indicated as red-dots) interactions.

The mechanistic proposal illustrated in Fig.11 is qualitatively consistent with several experimental observations. First, as mentioned above, increasing the separation between Arg sidechains does not change the overall phase of the peptide/lipid mixture but increases the lattice constant of the bicontinuous phase and reduces the degree of negative Gaussian curvature.<sup>21</sup> In the framework of Fig.11, with larger distances between Arg sidechains, the impact on the lipid distribution is expected to decrease. As a result, the enhancement of local positive principal curvature is less significant and therefore the magnitude of negative Gaussian curvature also decreases. Second, it has been shown that many antimicrobial peptides, which feature a combination of Lysine and hydrophobic residues, also stabilize the bicontinuous phase of lipids.<sup>22</sup> This is consistent with our mechanistic hypothesis in Fig.11: by introducing hydrophobic residues, the peptides are able to interact more strongly with the non-polar lipid tails and therefore lead to different lipid packings.

As a result, the combination of Lys and hydrophobic residues makes the peptides better resemble poly-Arg in terms of co-localization with anionic lipids and enhancement of local positive principal curvature, both of which are required for the stabilization of negative Gaussian curvature. Finally, we note that radial distribution functions in Fig.S3 indicate that Arg is able to interact with multiple lipids through multivalent interactions; this "cross-linking" effect helps enhance the local curvature, as reflected by the observation (Fig.6) that local positive curvature in the bicontinuous phase often far exceeds the spontaneous curvature of PS ( $\sim 0.07\text{nm}^{-1}$ ).<sup>37</sup> This is qualitatively consistent with the experimental observation that only poly-Arg peptides of length longer than 5 are able to stabilize the bicontinuous phase.<sup>7</sup>

## Conclusions

In this work, CG simulations with the BMW-MARTINI model are used to reveal the phase structure and spatial distribution of different components of cationic peptide(poly-Arg/Lys)/lipid(PE/PS) mixtures. Together with analysis of relevant systems at the atomistic level, these results lead to novel insights regarding factors that dictate the distinct phase behavior of such mixtures, especially concerning the key differences between poly-Arg and poly-Lys despite similar charge states.

The simulations reproduce the experimentally observed phases in the presence of poly-Arg and poly-Lys. The simulations demonstrate the importance of both peptide-phosphate-group and peptide-glycerol interactions on the phase behavior. In particular they suggest that peptide-glycerol interactions are the key to the difference in phase behavior with the two different peptides. The proposed mechanism is that poly-Arg forms strong effective interactions with lipids through both phosphate and glycerol groups, leading to a local segregation and co-localization of Arg and PS. All these factors promote regions of negative Gaussian curvature and therefore stabilize a bicontinuous phase. In the absence of this co-localization, which happens, for example, if the electrostatic interactions or glycerol-peptide interactions are made weaker, the inverted hexagonal phase is recovered. Although the roles of electrostatic interactions have been explored in previous experiments,

1  
2  
3 tal studies,<sup>5,7</sup> the impact of the glycerol-peptide interactions has not been tested experimentally.  
4 Using non-glycero phospholipids, we anticipate based on the current study that the lipid/peptide  
5 phase behavior depends less on whether poly-Arg or poly-Lys is present. Advanced spectroscopic  
6 techniques such as two-dimensional infrared spectroscopy<sup>39</sup> should be valuable for comparing  
7 Arg/Lys-lipid interactions with atomic resolution.  
8  
9

10 Collectively, the results of this work and previous experimental studies<sup>14,16,21,22</sup> highlight that  
11 the phase behavior of peptide/lipid mixtures is likely a balance of contributions from multiple  
12 groups of the underlying components.<sup>40</sup> Therefore, modifying the physicochemical nature of spe-  
13 cific component(s) may lead to either a qualitative or quantitative change in the resulting phase.  
14 This provides opportunities to experimentally fine-tune the properties of the peptides/polymers for  
15 specific applications. For computational studies to be able to quantitatively predict the impact of  
16 chemical modifications, additional simulations and/or theoretical studies are needed. For exam-  
17 ple, atomistic simulations are needed to better understand how various functional groups modulate  
18 the spontaneous curvature of lipids. In addition, more extensive simulations and theoretical stud-  
19 ies (e.g., with self-consistent-field-theory<sup>41</sup>) are needed to better quantify the phase diagram of  
20 peptide/lipid mixtures.  
21  
22

23 Finally, from a technical perspective, the current study supports the unique value of the BMW-  
24 MARTINI model in the analysis of systems that feature strong electrostatic interactions, although  
25 the results on poly-Lys also emphasize the potential subtlety of CG studies, where small changes  
26 in specific interactions leading to qualitatively different phases. In this regard, our work demon-  
27 strate that the combination of simulations at different resolutions is essential because they address  
28 different aspects of the problem and inform each other regarding the design of most revealing sim-  
29 ulations. CG simulations are used to simulate the phase behavior of peptide/lipid mixtures and  
30 allow a qualitative exploration of factors potentially important to the formation of a specific phase.  
31 The CG results stimulate targeted atomistic simulations, which are required to probe specific as-  
32 pects of amino acid/lipid interactions at the local level. Analysis of the atomistic simulations in  
33 turn leads to the design of altered/improved CG models to confirm the impact of certain features  
34  
35

on the phase behavior. We expect that the similar strategy is applicable to a broad set of problems that involve remodeling of biomembranes by peptides and proteins.

## Acknowledgement

The research was supported in part by National Science Foundation Grant CHE-0957285 to QC and CHE-1111835 to AY. Computational resources from the National Center for Supercomputing Applications at the University of Illinois and the Center for High Throughput Computing (CHTC) at UW-Madison are greatly appreciated; computations are also supported in part by National Science Foundation through a major instrumentation grant (CHE-0840494).

## Supporting Information Available

Additional simulation results with the MARTINI and Polarizable MARTINI models and additional analysis for the BMW-MARTINI simulations are included. This material is available free of charge via the Internet at <http://pubs.acs.org/>.

## References

- (1) McLaughlin, S.; Murray, D. Plasma Membrane Phosphoinositide Organization by Protein Electrostatics. *Nature* **2005**, *438*, 605–611.
- (2) Jiang, Y.; Ruta, V.; Chen, J.; Lee, A.; MacKinnon, R. The Principle of Gating Charge Movement in a Voltage-dependent K<sup>+</sup> Channel. *Nature* **2003**, *423*, 42–48.
- (3) Catterall, W. A. Ion Channel Voltage Sensors: Structure, Function and Pathophysiology. *Neuron* **2010**, *67*, 915–928.
- (4) Krepkly, D.; Mihailescu, M.; Freites, J. A.; Schow, E. V.; Worcester, D. L.; Gawrisch, K.; Tobias, D. J.; White, S. H.; Swartz, K. J. Structure and Hydration of Membranes Embedded with Voltage-sensing Domains. *Nature* **2009**, *462*, 473–479.

- (5) Schmidt, N. W.; Wong, G. C. L. Antimicrobial Peptides and Induced Membrane Curvature: Geometry, Coordination Chemistry, and Molecular Engineering. *Curr. Opin. Solid State Mater. Sci.* **2013**, In press.
- (6) Futaki, S.; Suzuki, T.; Ohashi, W.; Yagami, T.; Tanaka, S.; Ueda, K.; Sugiura, Y. Arginine-rich Peptides. *J. Biol. Chem.* **2001**, *276*, 5836–5840.
- (7) Schmidt, N.; Mishra, A.; Lai, G. H.; Wong, G. C. L. Arginine-rich Cell-penetrating Peptides. *FEBS Lett.* **2010**, *584*, 1806–1813.
- (8) Li, L.; Vorobyov, I.; Allen, T. W. Potential of Mean Force and pK Profile Calculation for a Lipid Membrane-exposed Arginine Side Chain. *J. Phys. Chem. B* **2008**, *112*, 9574–9587.
- (9) MacCallum, J. L.; Bennett, W. F. B.; Tielemans, D. P. Distribution of Amino Acids in a Lipid Bilayer from Computer Simulations. *Biophys. J.* **2008**, *94*, 3393–3404.
- (10) Yoo, J.; Cui, Q. Does Arginine Remain Protonated in the Lipid Membrane? Insights from Microscopic  $pK_a$  Calculations. *Biophys. J.* **2008**, *94*, L61–63.
- (11) Gleason, N. J.; Vostrikov, V. V.; Greathouse, D. V.; R. E. Koeppe II, Buried Lysine, but not Arginine, Titrates and Alters Transmembrane Helix Tilt. *Proc. Natl. Acad. Sci. USA* **2013**, *110*, 1692–1695.
- (12) Harms, M. J.; Schlessman, J. L.; Sue, G. R.; B. Garcia-Moreno E., Arginine Residues at Internal Positions in a Protein Are Always Charged. *Proc. Natl. Acad. Sci. USA* **2011**, *108*, 18954–18959.
- (13) Mitchell, D. J.; Steinman, L.; Kim, D. T.; Fathman, C. G.; Rothbard, J. B. Polyarginine Enters Cells More Efficiently Than Other Polycationic Homopolymers. *J. Pept. Res.* **2000**, *56*, 318–325.
- (14) Mishra, A.; Gordon, V. D.; Yang, L.; Coridan, R.; Wong, G. C. L. HIV TAT Forms Pores

1  
2  
3 in Membrans by Inducing Saddle-splay Curvature: Potential Role of Bidentate Hydrogen  
4 Bonding. *Angew. Chem. Int. Ed. Engl.* **2008**, *47*, 2986–2989.  
5  
6  
7  
8  
9

10 (15) Li, G.; Cui, Q. What Is So Special About Arg 55 in the Catalysis of Cyclophilin A? Insights  
11 from Hybrid QM/MM Simulations. *J. Am. Chem. Soc.* **2003**, *125*, 15028–15038.  
12  
13  
14

15 (16) Mishra, A.; Lai, G. H.; Schmidt, N. W.; Sun, V. Z.; Rodriguez, A. R.; Tong, R.; Tang, L.;  
16 Cheng, J.; Deming, T. J.; Kamei, D. T.; Wong, G. C. L. Translocation of HIV TAT Peptide  
17 and Analogues Induced by Multiplexed Membrane and Cytoskeletal Interactions. *Proc. Natl.  
18 Acad. Sci. USA* **2011**, *108*, 16883–16888.  
19  
20  
21

22 (17) Wender, P. A.; Galliher, W. C.; Goun, E. A.; Jones, L. R.; Pillow, T. H. The Design of  
23 Guanidinium-rich Transporters and Their Internalization Mechanisms. *Adv. Drug. Deliv. Rev.*  
24 **2008**, *60*, 452–472.  
25  
26  
27

28 (18) Wender, P. A.; Kreider, E.; Pelkey, E. T.; Rothbard, J.; VanDeusen, C. L. Dendrimetic Molec-  
29 ular Transporters: Synthesis and Evaluation of Tunable Polyguanidino Dendrimers that Fa-  
30 cilitate Cellular Uptake. *Org. Lett.* **2005**, *7*, 452–472.  
31  
32  
33  
34

35 (19) Masunov, A.; Lazaridis, T. Potentials of Mean Force between Ionizable Amino Acid Side  
36 Chains in Water. *J. Am. Chem. Soc.* **2003**, *125*, 1722–1730.  
37  
38  
39

40 (20) Vazdar, M.; Uhlig, F.; Jungwirth, P. Like-Charge Ion Pairing in Water: An Ab Initio Molec-  
41 ular Dynamics Study of Aqueous Guanidinium Cations. *J. Phys. Chem. Lett.* **2012**, *3*, 2021–  
42 2024.  
43  
44  
45

46 (21) Schmidt, N. W.; Lis, M.; Zhao, K.; Lai, G. H.; Alexandrova, A. N.; Tew, G. N.; Wong, G.  
47 C. L. Molecular Basis for Nanoscopic Membrane Curvature Generation from Quantum Me-  
48 chanical Models and Synthetic Transporter Sequences. *J. Am. Chem. Soc.* **2012**, *134*, 19207–  
49 19216.  
50  
51  
52  
53  
54  
55  
56  
57  
58  
59  
60

- (22) Schmidt, N. W.; Mishra, A.; Lai, G. H.; Davis, L. K., M. Sanders; Tran, D.; Garcia, A.; Tai, K. P.; McCray, P. B., Jr.; Ouellette, A. J.; Selsted, M. E.; Wong, G. C. L. Criterion for Amino Acid Composition of Defensins and Antimicrobial peptides based on geometry of membrane Destabilization. *J. Am. Chem. Soc.* **2011**, *133*, 6720–6727.
- (23) Wu, Z.; Cui, Q.; Yethiraj, A. A New Coarse-grained Model for Water: the Importance of Electrostatic Interactions. *J. Phys. Chem. B* **2010**, *114*, 10524–10529.
- (24) Wu, Z.; Cui, Q.; Yethiraj, A. A New Coarse-grained Force Field for Membrane-peptide Simulations. *J. Chem. Theory Comput.* **2011**, *7*, 3793–3802.
- (25) Marrink, S. J.; de Vries, A. H.; Mark, A. E. Coarse Grained Model for Semiquantitative Lipid Simulations. *J. Phys. Chem. B* **2004**, *108*, 750–760.
- (26) Monticelli, L.; Kandasamy, S. K.; Periole, X.; Larson, R. G.; Tieleman, D. P.; Marrink, S. J. The MARTINI Coarse-Grained Force Field: Extension to Proteins. *J. Chem. Theory and Comput.* **2008**, *4*, 819.
- (27) Yesylevskyy, S. O.; Schäfer, L. V.; Sengupta, D.; Marrink, S. J. Polarizable Water Model for the Coarse-grained MARTINI Force Field. *PLoS Comput. Biol.* **2010**, *6*, e1000810.
- (28) Hess, B.; Kutzner, C.; van der Spoel, D.; Lindahl, E. GROMACS 4: Algorithms for Highly Efficient, Load-balanced, and Scalable Molecular Simulation. *J. Chem. Theory Comput.* **2008**, *4*, 435–447.
- (29) Marrink, S. J.; Periole, X.; Tieleman, D. P.; de Vries, A. H. Comment on "On Using a Too Large Integration Time Step in Molecular Dynamics Simulations of Coarse-grained Molecular Models" by M. Winger, D. Trzesniak, R. Baron and W. F. van Gunsteren, *Phys. Chem. Chem. Phys.*, 2009, *11*, 1934. *Phys. Chem. Chem. Phys.* **2010**, *12*, 2254–2256.
- (30) Rand, R. P.; Fuller, N. L. Structural Dimensions and Their Changes in a Reentrant Hexagonal-lamellar Transition of Phospholipids. *Biophys. J.* **1994**, *66*, 2127–2138.

- 1  
2  
3 (31) Herce, H. D.; Garcia, A. E. Molecular Dynamics Simulations Suggest a Mechanism for  
4 Translocation of the HIV-1 TAT Peptide Across Lipid Membranes. *Proc. Natl. Acad. Sci.*  
5 **2007**, *104*, 20805–20810.  
6  
7 (32) Fuhrmans, M.; Marrink, S. J. Molecular View of the Role of Fusion Peptides in Promoting  
8 Positive Membrane Curvature. *J. Am. Chem. Soc.* **2012**, *134*, 1543–1552.  
9  
10 (33) Park, S.; Bardhan, J. P.; Roux, B.; Lee, M. Simulated X-ray Scattering of Protein Solutions  
11 Using Explicit-solvent Models. *J. Chem. Phys.* **2009**, *130*, 134114.  
12  
13 (34) Humphrey, W.; Dalke, A.; Schulten, K. VMD- Visual Molecular Dynamics. *J. Molec. Graph-*  
14 *ics* **1996**, *141*, 33–38.  
15  
16 (35) A. D. MacKerell Jr., et al. All-atom Empirical Potential for Molecular Modeling and Dynam-  
17 ics Studies of Proteins. *J. Phys. Chem. B* **1998**, *102*, 3586–3616.  
18  
19 (36) Klauda, J. B.; Venable, R. M.; Freites, J. A.; O'Connor, J. W.; Tobias, D. J.; Mondragon-  
20 Ramirez, C.; Vorobyov, I.; Jr, A. D. M.; Pastor, R. W. Update of the CHARMM All-atom  
21 Additive Force Field for Lipids: Validation on Six Lipid Types. *J. Phys. Chem. B* **2010**, *114*,  
22 7830–7843.  
23  
24 (37) Zimmerberg, J.; Kozlov, M. M. How Proteins Produce Cellular Membrane Curvature. *Nat.*  
25 *Rev. Mol. Cell Biol.* **2006**, *7*, 9–19.  
26  
27 (38) Yang, L.; Gordon, V. D.; Trinkle, D. R.; Schmidt, N. W.; Davis, M. A.; DeVries, C.;  
28 Som, A.; J. E. Cronan Jr.,; Tew, G. N.; Wong, G. C. L. Mechanism of a Prototypical Synthetic  
29 Membrane-active Antimicrobial: Efficient Hole-punching via Interaction with Negative In-  
30 trinsic Curvature Lipids. *Proc. Natl. Acad. Sci. USA* **2008**, *105*, 20595–20600.  
31  
32 (39) Woys, A. M.; Lin, Y. S.; Reddy, A. S.; Xiong, W.; de Pablo, J. J.; Skinner, J. L.; Zanni, M. T.  
33 2D IR Line Shapes Probe Ovispirin Peptide Conformation and Depth in Lipid Bilayers. *J.*  
34 *Am. Chem. Soc.* **2010**, *132*, 2832–2838.  
35  
36  
37  
38  
39  
40  
41  
42  
43  
44  
45  
46  
47  
48  
49  
50  
51  
52  
53  
54  
55  
56  
57  
58  
59  
60

- 1  
2  
3 (40) Sodt, A. J.; Pastor, R. W. Bending Free Energy from Simulation: Correspondence of Planar  
4 and Inverse Hexagonal Lipid Phases. *Biophys. J.* **2013**, *104*, 2202–2211.  
5  
6  
7 (41) Fredrickson, G. H. *The Equilibrium Theory of Inhomogeneous Polymers*; Oxford Science  
8 Publications: Oxford, UK, 2006.  
9  
10  
11  
12  
13  
14  
15  
16  
17  
18  
19  
20  
21  
22  
23  
24  
25  
26  
27  
28  
29  
30  
31  
32  
33  
34  
35  
36  
37  
38  
39  
40  
41  
42  
43  
44  
45  
46  
47  
48  
49  
50  
51  
52  
53  
54  
55  
56  
57  
58  
59  
60

1  
2  
3  
4  
5  
6  
7  
8  
9  
10  
11  
12  
13  
14  
15  
16  
17  
18  
19  
20  
21  
22  
23  
24  
25  
26  
27  
28  
29  
30  
31  
32  
33  
34  
35  
36  
37  
38  
39  
40  
41  
42  
43  
44  
45  
46  
47  
48  
49  
50  
51  
52  
53  
54  
55  
56  
57  
58  
59  
60

## Graphical TOC Entry

